Ab-initio vibrational properties of transition metal chalcopyrite alloys determined as high-efficiency intermediate-band photovoltaic materials

P. Palacios , I. Aguilera , P. Wahnón

Instituto de Energía Solar & Dpt. de Tecnologías Especiales, ETSI de Telecomunicación, UPM. Ciudad Universitaria s/n, 28040 Madrid, Spain
Instituto de Catálisis y Petroleoquímica, CSIC. Marie Curie 2, Cantoblanco, 28049 Madrid, Spain

Abstract

In this work, we present frozen phonon and linear response ab-initio research into the vibrational properties of the $CuGaS_2$ chalcopyrite and transition metal substituted $(CuGaS_2)M$ alloys. These systems are potential candidates for developing a novel solar-cell material with enhanced optoelectronic properties based in the implementation of the intermediate-band concept. We have previously carried out ab-initio calculations of the electronic properties of these kinds of chalcopyrite metal alloys showing a narrow transition metal band isolated in the semiconductor band gap. The substitutes used in the present work are the 3d metal elements, Titanium and Chromium. For the theoretical calculations we use standard density functional theory at local density and generalized gradient approximation levels. We found that the optical phonon branches of the transition metal chalcopyrite, are very sensitive to the specific bonding geometry and small changes in the transition metal environment.

Keywords: Chalcopyrite; Intermediate-band materials; Vibrational calculations

1. Introduction

Semiconductors in which transition metals (TM) substitute one or several atoms in the host material giving rise to a new band inside the semiconductor band gap, have recently been attracting a lot of attention. One of the main applications is spintronics. We have previously studied other novel applications based on the implementation of the intermediate band (IB) concept using III–V materials The IB concept is postulated as able to enhance the efficiency of photovoltaic (PV) cells. This new intermediate band must be isolated from the ordinary valence and conduction band of the host semiconductor in order to avoid fast de-excitation as a result of the interaction with phonons that are the subject of this work. The new band must also be a real band and not a level (an impurity, for example) so as to de-localise electron in the Intermediate Band and to avoid non-radiative recombination processes which can drastically reduce the efficiency of the solar cell. All of these requirements must be fulfilled in order to have an efficient light absorption and good quantum efficiencies. It is possible to obtain the optical absorption of the system, using quantum-mechanical calculations of the transition matrix elements between the corresponding band states. In our case we use the TM intermediate band to enhance the use of sub-band gap energy photons The IB concept has an ideal solar energy conversion limit of up to 63.2% at maximum concentration, higher than the 41% of normal single-junction cells. Transition metal-doped III–V materials based on GaAs or GaP have been the first candidates proposed by us to obtain this intermediate band. Other groups have presented other approaches derived from oxide compounds.

Chalcopyrite semiconductors of the I–III–VI_2 type such as $CuGaS_2$ have attracted a lot of attention as a result of their diverse structural, electrical and optical properties, which allow

applications in nonlinear optical devices, detectors, and solar cells Specifically $CuInSe_2$ chalcopyrite and its related compounds $Cu(InGa)(SSe)_2$ using thin-film technology are one of the most promising solutions for the production of an economically and competitive photovoltaic energy market. In the context of the use of thin-film technology to obtain high-efficiency solar-cell materials we have previously presented ab-initio structure calculations for the $CuGaS_2$ chalcopyrite partially substituted with TM atoms such as Ti, V, Cr or Mn to see whether some of these systems could provide an intermediate-band material

These calculations have been made using standard density functional theory (DFT) methods and advanced theory levels beyond DFT, such as Exact Exchange or Hubbard-type methods in order to determine the intermediate-band position. The Ti and Cr-substituted systems seem to be the most suitable materials to give an intermediate-band material with the desired properties, as well as being feasible from the thermodynamic point of view. The V and Mn systems give rise to half-metal structures with applications in spintronics [15].

In this work, first principles theoretical research into both the phonon and phonon density spectra of this novel TM intermediate-band semiconductor $Cu_4Ga_3S_8M$, M = Ti or Cr have been studied using the frozen phonon approximation [16,17]. To assess the validity of our results we present first, equivalent phonon ab-initio calculations for the $CuGaS_2$ host semiconductor. The calculated local density (LDA) and generalized gradient approximation (GGA) phonon dispersion curves for the chalcopyrite system are in very good agreement with experimental Raman and infrared data [18–20] and ab-initio results at the Γ point [21]. This vibrational spectra study can be used to calculate the phonon contribution to the free energy balance of formation and assess the thermodynamic viability.

2. Models and methods

I–III–VI_2 type chalcopyrite semiconductors crystallize in the space group I-42d, number 122, with four formula units in each unit cell. It is a ternary analog of the diamond structure and essentially a distorted superstructure of zinc-blende in the z direction. One of the face cubic center sublattices is made up of an equal number of I and III type atoms, and the other one of the VI type atoms. Like the atoms in zinc-blende structure, each constituent atom in these ternary compounds is tetrahedrally coordinated to four neighboring atoms. This coordination results in two different I–VI and III–VI bond lengths which produces the aforementioned tetrahedral distortion and deformation of the unit cell, characterized by the quantity $n = c / a$. The unit vectors of the chalcopyrite primitive cell are (**a**,0,0), (0,**a**,0), (**a** / 2,**a** / 2,**c** / 2). The cations are located at 4a and 4b Wyckoff positions while anions are located at 8d.

The unit cell used for the substituted alloy in all calculations in this work has been constructed from the vectors (**a**,**b**,**c**) of the tetragonal chalcopyrite cell according to **a'** = (**a** + **b** + **c**) / 2, **b'** = (**a** + **b** − **c**) / 2 and **c'** = **b** − **a**. The resulting structure has 16 atoms in the unit cell with one Gallium atom replaced by a transition metal M. This $Cu_4Ga_3S_8M$ system is the primitive of a centered monoclinic lattice which has a C2 symmetry. For Titanium, the shortest M–M distance is ≈ 6.6 Å.

The first calculations of the electronic structure for the series of ternary Cu-based chalcopyrites using an ab-initio DFT approach were presented by Jaffe and Zunger We have carried out spin-polarized electronic structure DFT calculations at the GGA PW91 level using the plane-wave VASP code with ultrasoft potentials and a plane wave basis set with an energy cutoff of 233.7 eV. The Brillouin zone was sampled using 6×6×6 Monkhorst–Pack grids with 112 irreducible *k*-points including the *Γ* point in the calculations. Unconstrained atomic relaxations were made using convergence parameters up to 0.04 eV/Å for atomic forces.

In the phonon calculation we need to relax the nucleus to a mechanical equilibrium in which the forces vanish. After that we compute the interatomic force constant matrix. This is achieved by carrying out a conjugate gradient minimization of the total energy with respect to the ion position. In our calculations all the atomic coordinates were relaxed until the largest force components went below 0.001 eV/Å and the stress tolerance less than 0.1 GPa. Less tolerance is necessary for the phonon force than the force tolerance for band energy minimization in order to obtain converged results (0.04 eV/Å is enough for band diagram case). Finally we obtained the vibrational frequencies by computing the second derivative of the Bohr–Oppenheimer energy in respect to their nuclear positions. We have used the frozen-phonon method where the phonons are calculated from the dynamical matrix. This matrix contains the spring constants, which represents the interaction between the atom pairs in real space.

To obtain these spring constants, we create supercells at different sizes and checking that the forces vanish for distant neighbours. For the $CuGaS_2$ we have made supercells of up to 3×3×3 (216 atoms). For the $Cu_4Ga_3S_8M$ with M = Ti or Cr, we have made supercells of up to 3×3×2 (288 atoms). In order to obtain a free energy balance of formation we must calculate other systems such as $CuCrS_2$, $Cu_{2/3}TiS_2$ and Cu [26]. The first one is a 4-atom system where we use a 3×3×3 supercell (108 atoms). The second one, the $Cu_{2/3}TiS_2$ has 11 atoms in the unit cell and we use a 2×2×1 supercell (44 atoms). For Copper, 1 atom in the unit cell, we use a 3×3×3 supercell.

To obtain the vibration eigen-frequencies in the supercell, the interatomic force constant must be determined first. When a vibration is produced in the lattice, an atom *i* in a primitive cell *l*, of bulk M_i, is displaced in the balance by *u*(*li*). The force in each atom is given as the second derivative from total energy. $\phi_{\alpha\beta}\left(ll'ii'\right) = -\frac{\partial^2 E}{\partial\mu_\alpha(li)\partial\mu_\beta\left(l'i'\right)}$. Here α,β are polarization vectors and *i* and *i'* are the positions of the atoms in the unit cells *l* and *l'* respectively. The vibration mode is defined as a movement: $F_{l,i} = -M_i\omega^2\mathbf{u}(l,i)$. We make small displacements of some atoms inside the supercell in different directions, and then the forces produced on the others atoms of the supercell are calculated.

Table 1
Lattice constant (in Å) ab-initio calculations for the host and substituted semiconductor chalcopyrites compared to experimental value

	LDA	GGA
$CuGaS_2$	5.22 (1.98)	5.34 (1.98)
$Cu_4Ga_3S_8Cr$	5.20 (1.99)	5.33 (1.99)
$Cu_4Ga_3S_8Ti$	5.24 (1.99)	5.36 (1.99)

The tetragonal distortion is shown in brackets.

After that, it is necessary to make a fast fourier transform to the dynamical matrix for each **k**, $D(\mathbf{k})$

$$D_{\alpha\beta}\left(ii'|\mathbf{k}\right) = \sum_{l} \frac{1}{\sqrt{M_i M_{i'}}} \phi_{\alpha\beta}\left(0l'ii'\right) e^{i\mathbf{k}}[x_l - x_0]$$

and finally the secular equation is solved: $-\omega^2\phi = D(\mathbf{k})\phi$. The phonon dispersion diagram is represented in specific parts of the crystal Brillouin zone. For $CuGaS_2$, GGA linear response phonon calculations have been calculated using the ABINIT code [27]. To obtain the phonon density of states we use a uniform Monkhorst–Pack Brillouin sampling of $11\times11\times11$ (666 points) in order to obtain a good integral over the whole Brillouin zone.

3. Results

Because there are no experimental data for the $Cu_4Ga_3S_8M$ alloys, we have calculated first the LDA and GGA phonon spectrum of pure binary compound $CuGaS_2$ in the chalcopyrite structure, in order to assess our results with available experimental Infrared and Raman data and other theoretical data for the host compound. We have previously presented ab-initio

Table 2
$CuGaS_2$ vibrational frequency calculation results (in cm^{-1}) compared to experimental data (Ref. [19], Ref. [20]) and ab-initio data values (Ref.)

Symmetry	LDA	GGA (LR)	GGA			
B_2^1 TO	375	348	365	368	368	355
	374	343	339	No	No	342
E^1LO	365	340	335	384	387	367
E^1TO	365	340	330	363	364	346
B_1^1	358	335	329	358	358	330
E^2LO	348	319	323	352	348	328
E^2TO	348	319	309	332	332	314
A_1	328	300	293	312	312	290
B_2^2TO	324	291	284	262	258	235
	268	258	263	No	No	269
E^3LO	307	268	257	276	271	241
E^3TO	307	268	249	262	258	236
B_1^2	211	197	196	203	202	196
E^4TO	190	171	162	156	165	162
E^4LO	190	170	162	156	165	162
E^5TO	122	117	123	No	116	117
E^5LO	122	117	112	No	116	117
B_1^3	118	107	111	97	99	99
B_2^3TO	107	99	111	95	95	99
E^6TO	88	82	76	74	74	83
E^6LO	88	82	76	74	74	83

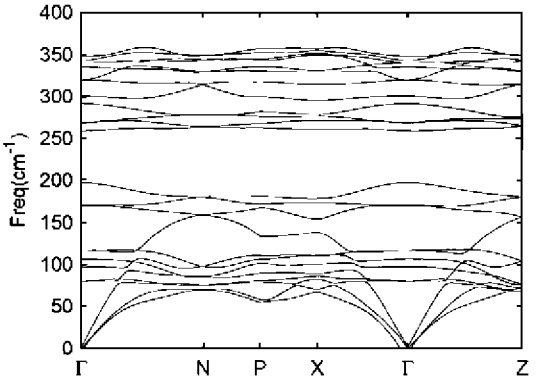

Fig. 1. $CuGaS_2$ phonon dispersion diagram calculated using the GGA method.

structure calculations for the $CuGaS_2$ host chalcopyrite and for the partially substituted cases with Titanium and Chromium in order to ascertain whether some of these systems could provide an intermediate-band material. The calculated lattice parameters a and distortion parameter n are shown and compared with experimental data in Table 1.

The optimized lattice parameter constants for $CuGaS_2$ for LDA calculation are 5.22 Å and for GGA calculations are 5.34 Å, compared to the experimental data 5.34 Å to 5.36 Å [28]. The lattice constants calculations agree very well with the experimental data, matching the GGA value exactly with the experiment and showing a lattice parameter compression of 2.2% for the LDA.

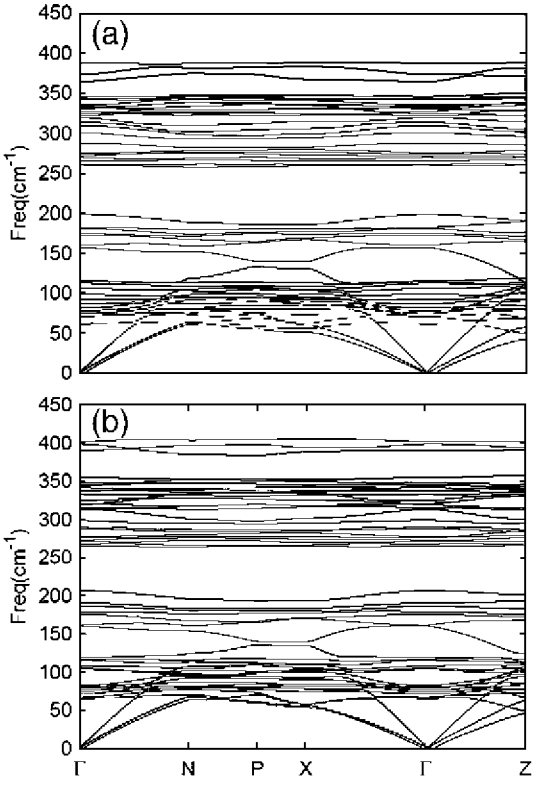

Fig. 2. $Cu_4Ga_3S_8M$ phonon dispersion diagram calculated using the GGA method for M=Ti (a) and Cr (b).

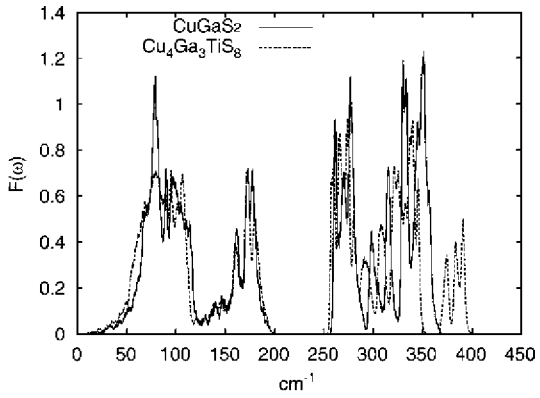

Fig. 3. $CuGaS_2$ and $Cu_4Ga_3S_8Ti$ GGA phonon density of states.

Phonon dispersion spectra results for the LDA and GGA calculations for the system are compared with available experimental data and LDA theoretical data at the Γ point. The primitive chalcopyrite cell has 8 atoms (24 modes of vibration). The group theory analysis for the zone centre of the chalcopyrite space group gives $1A_1$ and $3B_1$ normal modes that are Raman actives, and $3B_2$ and 6E which are Raman and Infrared actives. Our ab-initio calculations are in good agreement with this data except for the E_{LO} longitudinal optical phonon at the limit of the Γ-point where a macroscopic electric field of the long-range ion–ion interaction appears. This E_{LO} mode, which was previously degenerated with the E_{TO}, is modified by the field. We have not found LO–TO phonon splitting in the frozen-phonon calculations, but it does appear when we use the linear response method. The results exhibit smaller frequency values for the GGA case in all vibrational modes related to that of LDA. The GGA increases the lattice constant, which softens the phonon frequencies and worsens the results. The results compared with experimental and previously ab-initio data for the Γ point are shown in Table 2. It is possible to obtain the Γ point results by using the primitive cell, but in order to obtain the full dispersion phonon diagram it is necessary to use supercells. $2\times2\times2$, $3\times3\times2$ and $3\times3\times3$ supercells have been used to obtain the full diagram. Fig. 1, shows the more accurate results for the GGA case.

Besides that, we determine the lattice dynamics and phonon density of states (PDOS) of the substituted chalcopyrite systems $Cu_4Ga_3S_8M$, M=Ti and Cr. The GGA diagrams for these two systems are shown in Fig. 2.

We see that the overall shape is retained compared to the chalcopyrite host system, especially in the shape of the acoustic modes of the new alloy structures that remains almost unchanged. However, in the optical branches of both quaternary systems, new additional isolated high-phonon optical modes appear in the main high symmetry direction of the whole Brillouin zone. This new branch is clearly shown in Fig. 3

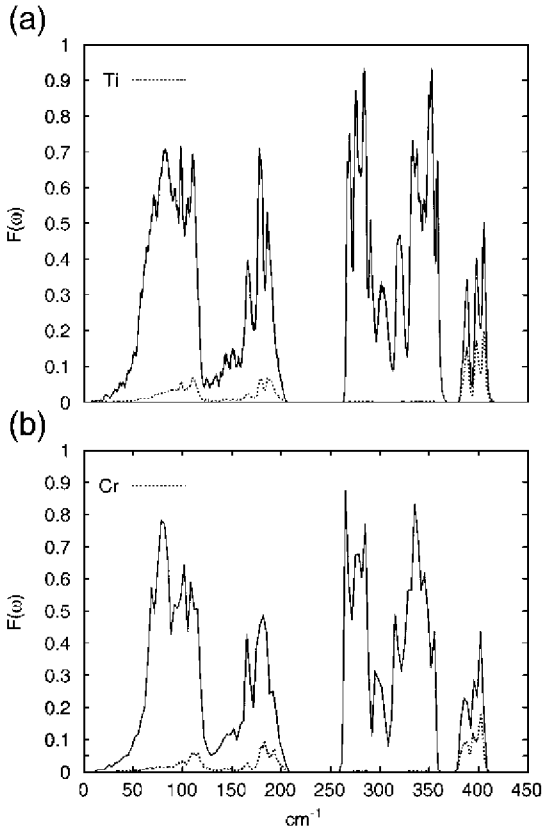

Fig. 4. $Cu_4Ga_3S_8M$ GGA phonon density of states including the projected metallic contribution for M=Ti (a) and Cr (b).

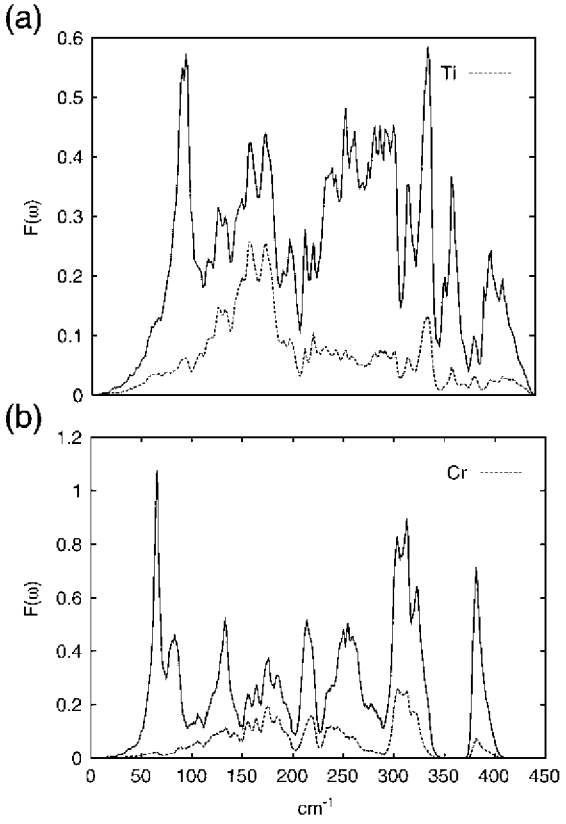

Fig. 5. $Cu_{2/3}TiS_2$ (a) and $CuCrS_2$ (b) GGA phonon density of states including the projected metallic contribution.

where the phonon density of states is compared for both the $CuGaS_2$ and the $Cu_4Ga_3S_8Ti$ systems.

We have also calculated the metal contribution to this phonon density of states. The contributions are shown in Fig. 4 (a–b) for Titanium and Chromium. From 50 cm^{-1} to 200 cm^{-1} there appear small contributions of these metals to the phonon spectra. Metal phonon density does not appear in the frequency range from 250 cm^{-1} to 350 cm^{-1} and finally the new optical branch is mainly made up of the metal substituents. If we define as optical gap, the difference between the last frequency attributed to the host semiconductor and the beginning of the normal modes, mainly as a result of the transition metal, we find the values of 28 cm^{-1} and 35 cm^{-1} for Titanium and Chromium respectively. Since there is a greater mass difference between Ti and Ga than Cr and Ga, could be expected that these new optical vibrational modes have a wider phonon optical gap for Titanium. The reason for these values is attributed to the shorter $Cu_4Ga_3S_8Cr$ lattice parameters, which increase the frequencies.

Because of the main goal in obtaining this frequencies is the inclusion of the vibrational entropy contribution to the free formation energy for $Cu_4Ga_3S_8M$, as we previously presented for III–V alloy systems it is necessary to evaluate the rest of the systems which appears in the reactions of $CuCrS_2 + 3CuGaS_2 \rightarrow Cu_4Ga_3CrS_8$ for Cr and $3CuGaS_2 + Cu_{2/3}TiS_2 + 1/3Cu \rightarrow Cu_4Ga_3TiS_8$ and Ti.

$CuCrS_2$, $Cu_{2/3}TiS_2$ and Cu metal systems have been evaluated and we shown the phonon density of states with the metal contribution for the ternary systems in Fig. 5.

4. Conclusions

We have calculated accurate ab-initio LDA and GGA phonon dispersion relationships and density of states for $Cu_4Ga_3S_8M$, M=Ti and Cr alloy semiconductor systems, using the frozen phonon method. We have also calculated first, with similar accuracy, the phonon spectra of the host semiconductor $CuGaS_2$ using the frozen phonon and the linear response methods and compared them with experimental data in order to validate our quaternary systems results. We found, that especially in GGA, ab-initio calculations are in very good agreement with the experimental data. The Ti and Cr diluted semiconductor compounds present in all cases result in fewer degenerate phonon curves than the host semiconductor. The acoustic $CuGaS_2$ phonon modes could easily be identified with that corresponding to the substituted alloy systems. However, additional high vibration modes have been found as a result of the metals in the whole Brillouin zone for the new optical branches of the two substituted semiconductor compounds studied. We found that these optical phonon branches of the transition metal chalcopyrite, are very sensitive to the specific bonding geometry and to the small changes in the transition metal environment. These features appear mainly for the optical phonon branches, showing the differences between Titanium and Chromium due to the degree of distortion in the structure as compared to the host chalcopyrite.

Acknowledgements

This work has been supported by the Consolider Ingenio 2010 program through the GENESIS-FV(CSD2006-0004) project and the CALIBAND(MAT2006-10618) project of the Spanish Ministry of Education and Science and from the Community of Madrid NUMANCIA-MA(S-05050/ENE/0310) Research Programme. Authors thankfully acknowledge the computer resources provided by the CESVIMA Supercomputer Centre.

References

P. Wahnón, C. Tablero, Phys. Rev., B 65 (2002) 165115.
P. Wahnón, P. Palacios, J.J. Fernández, C. Tablero, J. Mater. Sci. 40 (2005) 1383.
P. Palacios, J.J. Fernández, K. Sánchez, J.C. Conesa, P. Wahnón, Phys. Rev., B 73 (2006) 085206.
A. Luque, A. Martí, Phys. Rev. Lett. 78 (1997) 5014.
I. Aguilera, P. Palacios, P. Wahnón, Thin Solid Films (2007), doi:10.1016/j.tsf.2007.12.085.
K.M. Yu, W. Walukiewicz, J. Wu, W. Shan, J.W. Beeman, M.A. Scarpulla, O.D. Dubon, P. Becla, Phys. Rev. Lett. 91 (2003) 246403.
A.M. Gaber, J.R. Tuttle, D.S. Albin, A.L. Tennant, M.A. Contreras, in: R. Noufi (Ed.), 12th NREL photovolaic program review AIP Conf. Proc. No. 306, AIP, New York, 1994, p. 59.
R.W. Birkmire, E. Eser, Annu. Rev. Mater. Sci. 27 (1997) 625.
J. Hedstrom, H. Ohlsen, M. Bodengard, A. Kylner, L. Stolt, D. Hariskos, M. Runckh, H.W. Schock, Proceedings of the 23rd IEEE Photovoltaic Specialist Conference, IEEE, New York, 1993, p. 364.
P. Palacios, K. Sánchez, J.C. Conesa, P. Wahnón, Phys. Status Solidi (a) 203 (2006) 1395.
P. Palacios, K. Sánchez, J.C. Conesa, J.J. Fernández, P. Wahnón, Thin Solid Films 515 (2007) 6280.
J.F. Dobson, G. Vignale, M.P. Das (Eds.), Electron density functional theory. Recent Progress and New Directions, Plenum, New York, 1998.
J.J. Fernández, C. Tablero, P. Wahnón, Int. J. Quantum Chem. 91 (2003) 157.
S.L. Dudarev, G.A. Botton, S.Y. Savrasov, C.J. Humphreys, A.P. Sutton, Phys. Rev., B 57 (1998) 1505.
S. Picozzi, Y. Zhao, A. Freeman, B. Delley, Phys. Rev., B 66 (2002) 205206.
K. Kunc, R.M. Martin, Phys. Rev. Lett. 48 (1982) 406.
K. Parlinski, Z.Q. Li, Y. Kawazoe, Phys. Rev. Lett. 21 (1997) 4063.
F.W. Ohrendorf, H. Haeuseler, Cryst. Res. Technol. 34 (1999) 339.
W.H. Koschel, M. Bettini, Phys. Stat. Sol., B 72 (1975) 729.
J. Gonzalez, B.J. Fernandez, Phys. Rev., B 46 (1992) 15092.
M. Akdogan, R. Eryigit, J. Phys. Cond. Mater. 14 (2002) 7493.
J.E. Jaffe, A. Zunger, Phys. Rev., B 28 (1983) 5822.
G. Kresse, J. Hafner, Phys. Rev., B 47 (1993) RC558;
G. Kresse, J. Furthmüller (Eds.), Phys. Rev., B, 54, 1996, p. 11169;
G. Kresse, J. Hafner, J. Phys.: Condens. Mater. 6 (1994) 8245.
N. Le Nagard, G. Collin, O. Gorochov, Mat. Res. Bull. 14 (1979) 1411.
N. Le Nagard, O. Gorochov, G. Collin, Mat. Res. Bull. 10 (1975) 1287.
I.K. Suh, H. Ohta, Y. Waseda, J. Mater. Sci. 223 (1988) 1.
X. Gonze, J.M. Beuken, R. Caracas, F. Detraux, M. Fuchs, G.-M. Rignanese, L. Sindic, M. Verstraete, G. Zerah, F. Jollet, M. Torrent, A. Roy, M. Mikami, Ph. Ghosez, J.-Y. Raty, D.C. Allan, Comp. Mater. Sci. 25 (2002) 478.
H. Hahn, G. Frank, W. Klinger, G. Storger, Z. Anorg. Chem. 271 (1983) 153;
H.W. Spiess, U. Haeberlen, G. Brandt, A. Rauber, J. Schneider (Eds.), Phys.Status Solidi, B, 62, 1974, p. 183;
S.C. Abrahams, J.L. Bernstein, J. Chem. Phys. 59 (1973) 5415.
P. Palacios, P. Wahnón, S. Pizzinato, J.C. Conesa, J. Chem. Phys. 124 (2006) 014711.